Synthesis and characterization of a new TiZrHfNbTaSn high-entropy alloy exhibiting superelastic behavior

J.J. Gao, Philippe Castany, Thierry Gloriant

Synthesis and characterization of a new TiZrHfNbTaSn high-entropy alloy exhibiting superelastic behavior

J.J. Gao, P. Castany, T. Gloriant*

Univ Rennes, INSA Rennes, CNRS, ISCR UMR 6226, 35000 Rennes, France

*Corresponding author: e-mail: Thierry.Gloriant@insa-rennes.fr

Abstract

In this study, a new single-phase bcc $Ti_{35}Zr_{35}Hf_{15}Nb_5Ta_5Sn_5$ high-entropy alloy (HEA) was developed and investigated by means of cyclic tensile tests, transmission electron microscopy (TEM), electron back-scattered diffraction (EBSD) and in situ synchrotron X-ray diffraction (SXRD). The alloy reveals a superelastic behavior due to the reversible stress-induced martensitic transformation that occurs between the β phase and the α" phase. A high strain recovery of 3.8% is obtained by tensile test, which is attributed to the $<110>_\beta\{447\}_\beta$ recrystallization texture observed.

Keywords: high-entropy alloy; superelasticity; texture; martensitic transformation

The concept of high-entropy alloy (HEA) introduced in 2004 [1,2] is commonly defined as multicomponent alloys that contain at least five metallic elements varying in chemical composition from 5 at.% to 35 at.% [1,3]. In recent decades, HEAs have been drawing considerable attention due to their potentialities to acquire superior mechanical properties, including high strength, high work-hardening rate, good ductility…[1,3,4]. HEA definition is now controversial to describe multicomponent alloys and new names, such as complex concentred alloys, multi-principal element alloys or baseless alloys have appeared [4-7]. Nevertheless, the term high-entropy

alloy is still commonly used and it seems that this catchy name endures [~~4~~6]. Although numerous studies are reported in the literature on the development of new HEAs in its largest definition, more attention is now being increasingly paid to design and develop some “true” single phase solid solutions to probe and uncover fundamental mechanisms involving phase formation, defects and properties [5]. In the present study, we focused on the possibility to design a single phase HEA in which stress-induced transformation occurs. Recently, it was reported that stress-induced transformations, involving transformation induced plasticity (TRIP) and twinning induced plasticity (TWIP) effects, can occur in HEAs to improve the mechanical properties of face-centered cubic (fcc) CrMnFeCoNi alloys [~~6~~8] and body-centered cubic (bcc) TiZrHfNbTa alloys [9,10]. If such phase transformations could be reversible, one could obtain superelastic alloys, which are particularly suitable for the manufacture of biomedical devices. But only highly biocompatible elements should be used for the design of these potential superelastic HEAs that exclude fcc alloys due to the presence of toxic or allergenic elements (Cr, Co, Ni) and tend to favour bcc alloys with a similar metallurgy than~~In~~ metastable beta titanium-based alloys (bcc). The superelastic behavior of this kind of Ti-based alloys is due to the reversible stress-induced martensitic (SIM) transformation occurring between the parent bcc β phase and the C-centered orthorhombic α" martensitic phase that leads to an important strain recovery [11-23]. The question is therefore whether it is possible to design a superelastic biomedical HEA with optimized recovery strain. This represents a challenging topic especially since few studies exist in the literature about superelastic HEA [24], but with non-optimal biocompatibility due to the use of Al that is known to have neurological toxic effects [25,26]. In order to achieve this goal, the equiatomic TiZrHfNbTa composition is switched to (Ti-Zr)-riched non-equiatomic composition,

since TiZrHfNbTa was revealed to display a stable bcc structure at room temperature, which does not allow to activate a stress-induced martensitic phase transformation mechanism [27,28]. Consequently, a new single-phase metastable β $Ti_{35}Zr_{35}Hf_{15}Nb_5Ta_5Sn_5$ HEA with only non-toxic elements was developed for biomedical applications in this study. Cyclic tensile tests, transmission electron microscopy, electron back-scattered diffraction and in situ synchrotron X-ray diffraction experiments were conducted on this new HEA with the objective to characterize the SIM transformation and to evaluate its superelastic performance.

Cold crucible levitation melting (CCLM) technique under argon atmosphere was employed to obtain the $Ti_{35}Zr_{35}Hf_{15}Nb_5Ta_5Sn_5$ (at.%) ingot by using 99.95% pure titanium, 99.078% pure zirconium, 99.9% pure hafnium, 99.9% pure tantalum, 99.9% pure niobium, and 99.99% pure tin elements. The ingot was then cold-rolled into a 0.5 mm sheet, which represents a reduction of around 95% of the initial thickness. Dog-bone tensile specimens were thus machined from the cold-rolled sheet along the rolling direction into a normalized shape: 3 mm width, 0.5 mm in thickness and a gage length of 15 mm. In order to restore a fully recrystallized β microstructure, the cold-rolled tensile specimens were then solution treated under high vacuum (~10^{-7} mbar) above the β-transus temperature at 750°C for 30 min followed by water quenching. The β-transus temperature was determined by electrical resistivity measurement performed on a lamella sample by using the four-probe method under high vacuum (10^{-7} mbar) between room temperature and 950°C and with a heating/cooling rate of 5°C/min [12].

In order to observe the solution-treated alloy microstructure, transmission electron microscopy (TEM, JEOL 2100F) operating at 200 kV was used. TEM specimens were prepared through twin-jet electropolishing system with a solution of 4%

perchloric acid and 96% methanol (vol.%) at -25°C. Determination of the recrystallization texture of the solution-treated alloy was conducted by electron back-scattered diffraction (EBSD, Oxford HKL SEM system). EBSD sample was mechanically polished by colloidal silica suspension mixed with H_2O_2 solution.

The mechanical properties, and more particularly the superelastic recovery strain, of the solution treated $Ti_{35}Zr_{35}Hf_{15}Nb_5Ta_5Sn_5$ HEA was evaluated by cyclic tensile tests with a strain rate of $10^{-4}s^{-1}$. The tensile direction was chosen parallel to the cold rolling direction. An extensometer was used to measure precisely the strain of the specimen. The cyclic tensile tests consist in increasing the strain by step of 0.5% in successive loading-unloading cycles.

In situ synchrotron X-ray diffraction (SXRD) experiment was carried out at the ID-22 beamline of the European Synchrotron Radiation Facility (ESRF, Grenoble, France) with a 0.35453630Å wavelength. SXRD profiles were acquired during a cyclic tensile test (at the rate of $10^{-4}s^{-1}$) with strain increments of 0.5% until 5% of strain during each loading and unloading condition. Nine-channel detector was employed to collect transmitted diffracted beams from $2\theta=6°$ to $2\theta=20°$ for each cycle.

Fig.1(a) shows the electrical resistivity curve obtained from the cold-rolled $Ti_{35}Zr_{35}Hf_{15}Nb_5Ta_5Sn_5$ alloy between 400°C and 950°C during a heating/cooling cycle. The β-transus temperature was evaluated at about 650°C in the present case. This measurement was thus used to choose the solution treatment temperature at 750°C. Fig.1(b) shows the initial SXRD profile with the typical $(110)_\beta$, $(002)_\beta$, $(112)_\beta$, $(220)_\beta$, $(013)_\beta$ diffracted beta peaks for the solution treated $Ti_{35}Zr_{35}Hf_{15}Nb_5Ta_5Sn_5$ HEA. A typical bright-field TEM image is presented in Fig.2(a) to reveal the recrystallized microstructure. Fig.2(b) and Fig.2(c) are the corresponding electron diffraction patterns on the $[113]_\beta$ and $[111]_\beta$ zone axes, respectively, confirm the

presence of the β phase only without any nano-scaled precipitate. A very refined equiaxed β-grain microstructure can thus be observed with a grain size not exceeding 1 μm. On the other hand, the recrystallization texture of the alloy was investigated by EBSD. Fig.2(d) presents a typical EBSD-IPF map for the rolling direction (RD) with the color code of the crystallographic orientations. The average grain size was evaluated to be 0.5 ± 0.4 μm. The orientation distribution function (ODF) has been calculated (available as supplementary figure, S.1) and the resultant inverse pole figures (IPF) are shown in Fig.2(e) and Fig.2(f) along the rolling direction (RD) and the normal direction (ND), respectively. As it can be seen, only a predominant $<110>_{\beta}\{447\}_{\beta}$ texture is detected meaning that most of grains are oriented to the $<110>_{\beta}$ direction parallel to the rolling and tensile directions.

In order to evaluate the superelastic performance of the present $Ti_{35}Zr_{35}Hf_{15}Nb_5Ta_5Sn_5$ alloy, cyclic loading/unloading tensile tests were carried out at room temperature. Fig.3 displays the typical cyclic engineering stress-strain curve obtained. It can be noted that the alloy has a relatively low ductility since the elongation at break does not exceed 5% of strain. On this cyclic tensile curve, a superelastic behavior can be evidenced due to the presence of hysteresis between loading and unloading curves, which are associated with the occurrence of a reversible SIM transformation between the parent β phase and the martensitic α" phase as in conventional Ti-based bcc alloys [11-13]. The maximum recovery strain, which is highlighted by the bold cycle on the tensile curve, can be evaluated at 3.8 %. In conventional beta-type superelastic titanium-based alloys, such a maximum recovery strain can also be reached in the case of very refined β-grain size microstructure as in the present case. Indeed, we showed in a recent work carried out on a $Ti_{66}Zr_{20}Nb_{12}Sn_2$ alloy composition that a reduced grain size is an important

parameter which impedes the trapping of the martensitic phase, and thus allows a better reversibility of the stress-induced martensitic transformation [13]. However, reduced grain size (<1µm) can only be obtained after a short-time recrystallization treatment just above the β-transus temperature (2 min at T_β+10°C). On the contrary, a reduced grain size can be directly obtained after a more conventional recrystallization treatment (30 min at T_β+100°C) with the present HEA alloy. The sluggish diffusion effect reported from HEAs [3,7,29] can explained the advantageous slow grain growth observed in the present case and allows to retain more easily sub-micrometric grain size.

In order to unambiguously evidence the SIM transformation occurring in the present alloy, an in situ SXRD study under the same cyclic loading/unloading tensile test was conducted. Fig.4(a) and (b) displays the SXRD profiles from initial to 4.5% of strain within the restricted 2θ=7.6°~8.8° angle range to reveal the evolution of the most intense β phase peak and SIM α" martensitic phase peaks during each loading and after unloading cycle, respectively. Fig.4(c) highlights the evolution of the SIM transformation during loading by the evolution of the relative intensity of $(110)_\beta$ peak (that is the ratio of the current intensity of the peak by the initial intensity of the same peak). To ensure a better readability, the intensity of the $(020)_{\alpha''}$ peak near 7.8° is zoomed 10 times on loading in Fig.4(a). Below 1.0% of applied strain, it can be noticed in Fig.4(a) that the $(110)_\beta$ peak shifts to the left when the strain increases, indicating the elongation of lattice parameter of the β phase on loading and returns back to its initial position after unloading. The deformation is then purely elastic below 1.0% of applied strain. The $(002)_{\alpha''}$, $(020)_{\alpha''}$ and $(111)_{\alpha''}$ martensitic peaks start to be detected from 1.0% of applied strain. This observation is in good agreement with the cyclic tensile curve in which the hysteresis start to be detected at the same

applied strain. It can then be deduced that the critical stress inducing the martensitic transformation is about 550 MPa for this alloy. With applied strain increasing from 1.0% to 4.5% on loading (Fig.4(a)), the intensity of the SIM $(002)_{\alpha''}$, $(020)_{\alpha''}$, $(111)_{\alpha''}$ peaks becomes stronger while the intensity of the $(110)_{\beta}$ peak decreases continuously (Fig.4(c)). On the other hand, it can be observed after unloading (Fig.4(b)) that the only detected peak is the one corresponding to the β phase. Consequently, the reversible SIM α" transformation is thus clearly evidenced by this in situ SXRD experiment.

It is well known that the lattice correspondence between β and SIM α" phases can be expressed as follows: $[100]_{\alpha''}$-$[100]_{\beta}$, $[010]_{\alpha''}$-$[011]_{\beta}$, $[001]_{\alpha''}$-$[0\text{-}11]_{\beta}$ [9,17-20]. In this system, the parent cubic β phase can thus transform into orthorhombic α" martensite crystal with 6 equiprobable lattice correspondence variants. However, when the α" martensite is stress-induced, a selection of variants occurs to promote the one leading to the maximum of transformation strain among the 6 ones in order to best accommodate the applied deformation strain. Thus, the maximum transformation strain, ε_{hkl}, induced by the lattice distortion due to the martensitic transformation from β phase to orthorhombic α" phase can be calculated for any direction as a function of lattice parameters of both phases [22,23]. In the present alloy, the recrystallization texture analysis revealed that most of β grains are oriented to the $<110>_{\beta}$ direction parallel to the tensile direction, which is known to be the best configuration to maximize the transformation strain [12-14,17,18,20,22,23]. Consequently, the maximum transformation strain value is given by: $\varepsilon_{110} = \frac{b_{\alpha''} - \sqrt{2}a_{\beta}}{\sqrt{2}a_{\beta}} \times 100$ (in %) in the present case, for which a_{β} corresponds to the lattice parameter of the β phase and $b_{\alpha''}$ corresponds to one of the lattice parameters of the α" phase. The in situ SXRD analysis carried out in the present study makes it possible to determine such cell

parameters from the profiles obtained on loading (Fig.4(a)). The following values were found: a_{β}=0.345 nm and $b_{\alpha''}$=0.519 nm. Therefore, the maximum theoretical transformation strain along the <110>$_{\beta}$ direction, ε_{110}, is calculated to be 6.3%. It is worth noting that this value of 6.3% is an ideal value and the experimental value found is much lower (3.8%). This is due to the fact that the maximum theoretical transformation strain is calculated for a perfect single-crystal without taking into account the real microstructure which contains grain boundaries, dislocations and other defects which are known to strongly influence the SIM α" transformation [11-12,30]. The present study shows however that higher strain recovery could be obtained by optimizing the chemical composition or the thermo-mechanical treatment making this kind of bcc HEA suitable for superelastic medical devices.

In summary, a new single phase bcc $Ti_{35}Zr_{35}Hf_{15}Nb_5Ta_5Sn_5$ HEA was elaborated in this work. After melting, the alloy was solution treated at 750°C for 30 min and then quenched in water. A very refined equiaxed β-grain microstructure (<1 μm) was observed by TEM. The recrystallization texture analysis by EBSD revealed that most of β grains were oriented to the <110>$_{\beta}$ direction parallel to the rolling direction, which corresponds to the tensile direction. By cyclic tensile tests, a superelastic behavior was evidenced and 3.8% of recoverable strain was obtained. This superelastic behavior is due to the reversible SIM transformation that occurs in this high-entropy alloy, which was evidenced by in situ SXRD experiments. The high recovery strain obtained is attributed to the <110>$_{\beta}${447}$_{\beta}$ recrystallization texture, which favors a maximum transformation strain along the <110>$_{\beta}$ crystallographic direction.

Acknowledgments

J.J. Gao acknowledges the China Scholarship Council (CSC) for his Ph.D financial support (No.2016-6329). The authors also acknowledge respectively the THEMIS and CMEBA platforms of the University of Rennes for providing access to the TEM and SEM-EBSD, and the ESRF (Grenoble, France) for the SXRD facilities.

References

[1] J.-W. Yeh, S.-K. Chen, S.-J. Lin, J.-Y. Gan, T.-S. Chin, T.-T. Shun, C.-H. Tsau, S.-Y. Chang, Adv. Eng. Mater. 6 (2004) 299–303.

[2] B. Cantor, I.T.H. Chang, P. Knight, A.J.B. Vincent, Mater. Sci. Eng. A 375–377 (2004) 213–218.

[3] M.-H. Tsai, J.-W. Yeh, Mater. Res. Lett. 2 (2014) 107–123.

[4] I. Basu, J.Th.M. DeHosson, Scripta Mater. 187 (2020) 148–156.

[5] K. Biswas, J.W. Yeh, P.P. Bhattacharjee, J.Th.M. DeHosson, Scripta Mater. 188 (2020) 54–58.

[6] E.P. George, D. Raabe, R.O. Ritchie, Nat. Rev. Mater. 4 (2019) 515–534.

[7] D.B. Miracle, O.N. Senkov, Acta Mater. 122 (2017) 448–511.

[8] B. Gludovatz, A. Hohenwarter, D. Catoor, E.H. Chang, E.P. George, R.O. Ritchie, Science 345 (2014) 1153–1158.

[9] L. Lilensten, J.-P. Couzinié, J. Bourgon, L. Perrière, G. Dirras, F. Prima, I. Guillot, Mater. Res. Lett. 5 (2017) 110–116.

[10] R.R. Eleti, M. Klimova, M. Tikhonovsky, N. Stepanov, S. Zherebtsov, Sci. Rep. 10 (2020) 13293.

[11] Y.L. Hao, Z.B. Zhang, S.J. Li, R. Yang, Acta Mater. 60 (2012) 2169–2177.

[12] J.J. Gao, I. Thibon, D. Laillé, P. Castany, T. Gloriant, Mater. Sci. Eng. A 762 (2019) 138075.

[13] J.J. Gao, I. Thibon, P. Castany, T. Gloriant, Mater. Sci. Eng. A 793 (2020) 139878.

[14] Y. Yang, P. Castany, M. Cornen, F. Prima, S.J. Li, Y.L. Hao, T. Gloriant, Acta Mater. 88 (2015) 25–33.

[15] Y.L. Hao, S.J. Li, S.Y. Sun, C.Y. Zheng, R. Yang, Acta Biomater. 3 (2007) 277–286.

[16] P. Castany, Y. Yang, E. Bertrand, T. Gloriant, Phys. Rev. Lett. 117 (2016) 245501.

[17] E. Bertrand, P. Castany, T. Gloriant, Acta Mater. 61 (2013) 511–518.

[18] M. Tahara, H.Y. Kim, T. Inamura, H. Hosoda, S. Miyazaki, Acta Mater. 59 (2011) 6208–6218.

[19] M. Besse, P. Castany, T. Gloriant, Acta Mater. 59 (2011) 5982–5988.

[20] P. Castany, A. Ramarolahy, F. Prima, P. Laheurte, C. Curfs, T. Gloriant, Acta Mater. 88 (2015) 102–111.

[21] P. Castany, D.M. Gordin, S.I. Drob, C. Vasilescu, V. Mitran, A. Cimpean, T. Gloriant, Shape Mem. Superelasticity 2 (2016) 18–28.

[22] E. Bertrand, P. Castany, Y. Yang, E. Menou, T. Gloriant, Acta Mater. 105 (2016) 94–103.

[23] H.Y. Kim, Y. Ikehara, J.I. Kim, H. Hosoda, S. Miyazaki, Acta Mater. 54 (2006) 2419–2429.

[24] L. Wang, C. Fu, Y. Wu, R. Li, X. Hui, Y. Wang, Scr. Mater. 162 (2019) 112–117.

[25] B. Mjöberg, E. Hellquist, H. Mallmin, U. Lindh, Acta Orthop. Scand. 68 (1997) 511–514.

[26] D. Zaffe, C. Bertoldi, U. Consolo, Biomaterials. 25 (2004) 3837–3844.

[27] O.N. Senkov, J.M. Scott, S.V. Senkova, F. Meisenkothen, D.B. Miracle, C.F. Woodward, J. Mater. Sci. 47 (2012) 4062–4074.

[28] J.-Ph. Couzinié, L. Lilensten, Y. Champion, G. Dirras, L. Perrière, I. Guillot, Mater. Sci. Eng. A 645 (2015) 255–263.

[29] K.-Y. Tsai, M.-H. Tsai, J.-W. Yeh**,** Acta Mater. 61 (2013) 4887–4897.

[30] F. Sun, S. Nowak, T. Gloriant, P. Laheurte, A. Eberhardt, F. Prima, Scr. Mater. 63 (2010) 1053–1056.

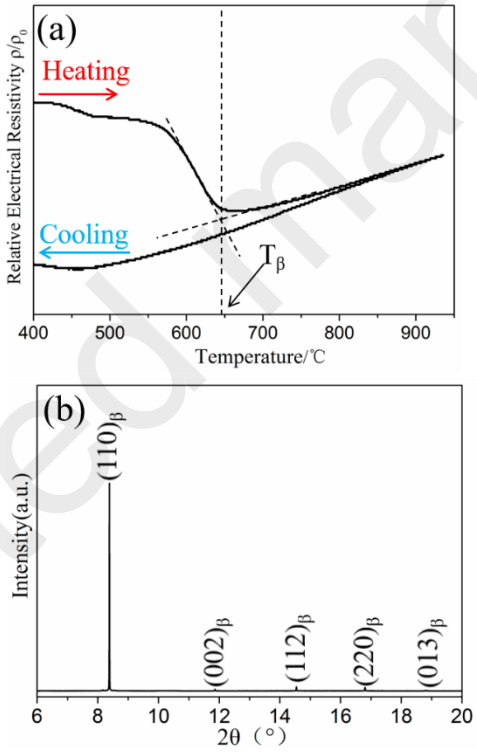

Fig.1 Resistivity curve of the cold-rolled $Ti_{35}Zr_{35}Hf_{15}Nb_5Ta_5Sn_5$ HEA between 400°C and 950°C (a) and SXRD profile of the solution treated alloy at 750°C for 30 min (b).

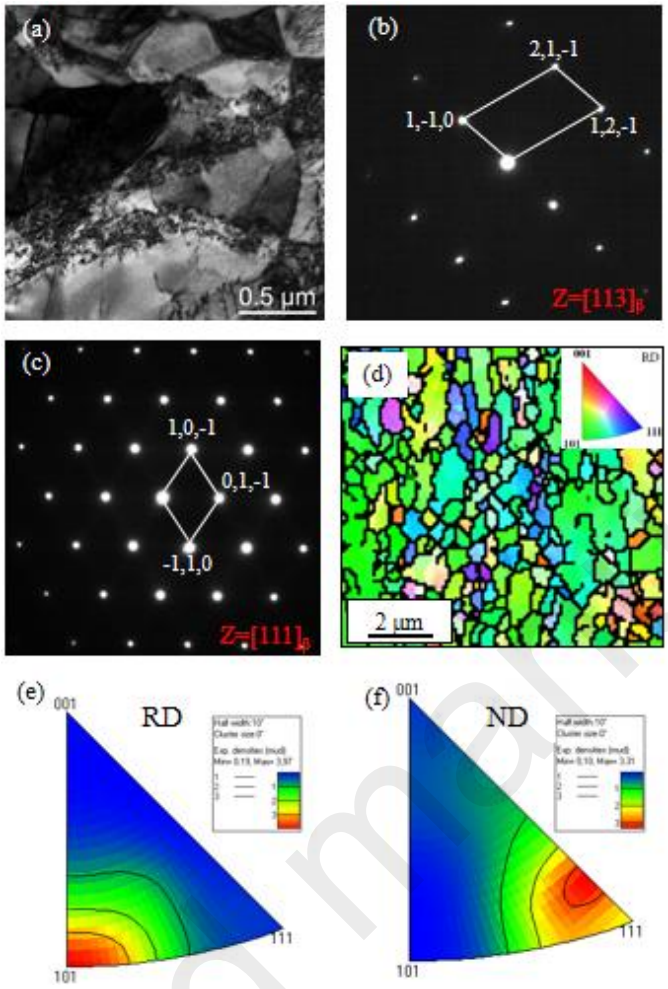

Fig.2 Bright-field TEM micrograph (a), and corresponding electron diffraction pattern on Z=[113]$_\beta$ (b) and Z=[111]$_\beta$ (c); EBSD-IPF map (d) with its color code, and RD (e) and ND (f) inverse pole figures of the solution-treated $Ti_{35}Zr_{35}Hf_{15}Nb_5Ta_5Sn_5$ HEA.

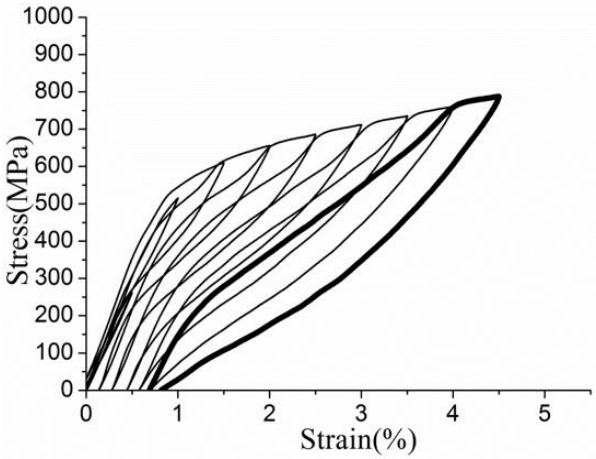

Fig.3 Engineering stress-strain curve of the $Ti_{35}Zr_{35}Hf_{15}Nb_5Ta_5Sn_5$ HEA obtained from cyclic tensile test at room temperature.

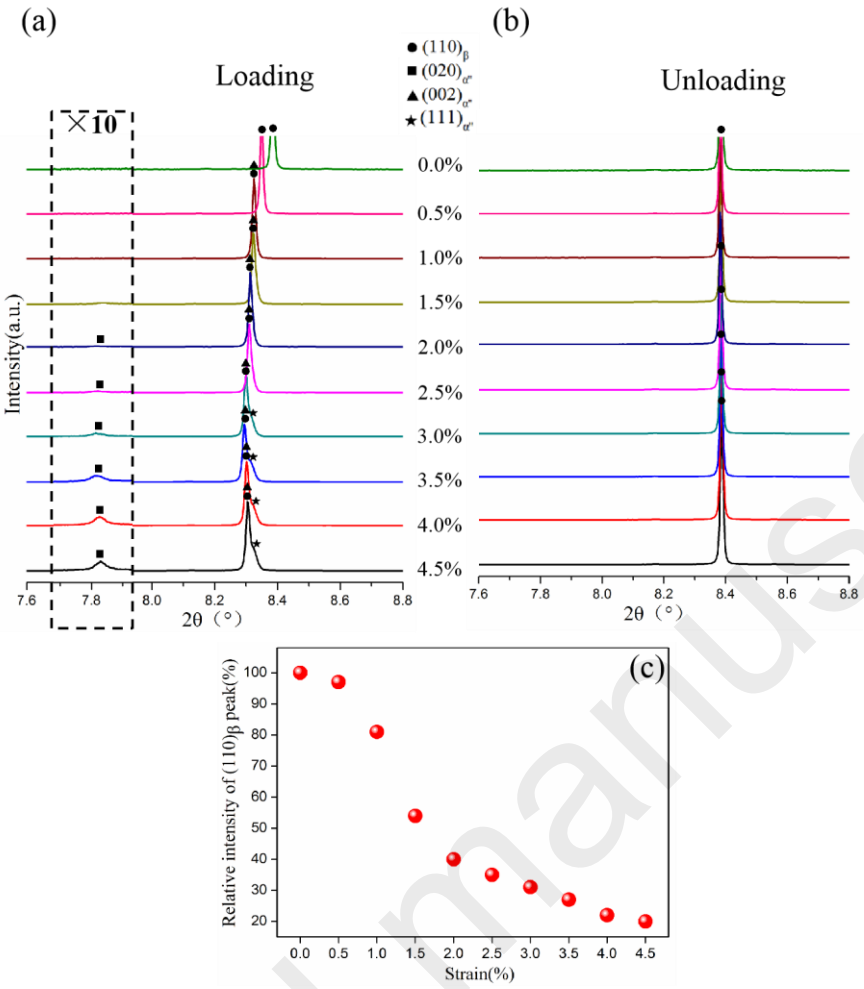

Fig.4 In situ SXRD profiles of the $Ti_{35}Zr_{35}Hf_{15}Nb_5Ta_5Sn_5$ HEA around 2θ=7.6° ~ 8.8° during cyclic tensile tests: on loading (a) and after unloading (b); evolution of relative intensity of the $(110)_\beta$ peak during loading as a function of the applied strain (c).

Graphical abstract